Article

# The Design of Superior Ethanol Gas Sensor Based on the Al-Doped NiO Nanorod-Flowers

Chen Wang, Xiaobiao Cui, Jiangyang Liu, Xin Zhou, Xiaoyang Cheng, Peng Sun, Xiaolong Hu, Xiaowei Li, Jie Zheng, and Geyu Lu

*ACS Sens.*, **Just Accepted Manuscript** • DOI: 10.1021/acssensors.5b00123 • Publication Date (Web): 17 Nov 2015

# The Design of Superior Ethanol Gas Sensor Based on the Al-Doped NiO Nanorod-Flowers

Chen Wang, Xiaobiao Cui, Jiangyang Liu, Xin Zhou, Xiaoyang Cheng, Peng Sun*, Xiaolong Hu, Xiaowei Li, Jie Zheng and Geyu Lu*

State Key Laboratory on Integrated Optoelectronics, College of Electronic Science and Engineering, Jilin University, Changchun 130012, People's Republic of China.

*KEYWORDS: Al-doped NiO, nanorod-flowers, solvothermal, gas sensor, ethanol*

**ABSTRACT:** The pure and Al-doped NiO nanorod-flowers with uniform sizes and well-defined morphologies were first time synthesized by a facile solvothermal reaction. As the gas sensing materials of MOS gas sensors, their sensing properties were investigated systematically. The results indicated that the 2.15 at% Al-doped NiO nanorod-flowers showed improved gas sensing properties compared to that of pure NiO nanorod-flowers. The incorporation of Al ions with NiO nanocrystals adjusts the carrier concentration, and induces the change of the oxygen deficiency and chemisorbed oxygen of NiO nanorod-flowers. Thus, the doping of $Al^{3+}$ into NiO nanorod-flowers should be a promising method for designing and fabricating the high performance gas sensor.

Presently, the researches related to gas sensor have attract constantly increasing interests since its extensive applications in industrial emission control, household security, environmental monitoring and disease diagnoses.[1, 2] Among various types of sensors, the resistive gas sensors which adopted metal oxide semiconductors as gas sensing materials have hold an central position due to their advantages of low-cost, high sensitivity, and simplicity of operation.[3-5] The operating mechanism is that the gas molecules are adsorbed or react with the surface chemisorbed oxygen species on the surfaces of the gas sensing material and thus induce the change of the sensor resistance.[6, 7] In this case, the gas sensing properties of the sensors are closely related to the morphology and composition of the gas sensing materials.[8-10] Therefore, it is essential to continually explore and innovate new functional gas sensing materials for achieving high-performance gas sensors.

Currently, various effective approaches, including the construction of complex and multidimensional nanostructures,[9] the loading of noble metal catalysts,[11] the formation of nanocomposites,[12] the aliovalent doping,[13, 14] and so on, have been utilized to improve the gas sensing properties of the metal oxide semiconductor (MOS) based gas sensors. Among them, incorporating aliovalent dopants into MOS nanocrystals is considered to be the most facile and reliable method to alter the structure, grain size, carrier concentration and distribution of oxygen component, thus, promoting the gas sensing performance of the MOS-based gas sensor. Nickel oxide (NiO) is an important p-type metal oxide semiconductor with excellent chemical and electric properties.[15-17] As gas sensing material,[18, 19] its sensitivity is relatively lower compared to n-type metal oxide semiconductors, such as $SnO_2$,[20] $In_2O_3$,[21] ZnO,[22] and $WO_3$.[23] However, NiO possesses a prominent catalytic activity for volatile organic compounds (VOC) oxidation.[24, 25] From this point of view, NiO should be a potential material terrace for designing and fabricating the high-performance VOC gas sensors. Therefore, some investigations into doping NiO nanocrystals with aliovalent ions (such as $Fe^{3+}$,[26] $Cr^{3+}$,[13] $W^{6+}$,[27] etc.) to enhance the gas sensing properties of NiO-based gas sensors have be carried out. Whereas, for systematically researching the sensitization mechanism and realizing effective detection of harmful or hazardous gases, these studies are far from enough.

On the basis of above mentioned, we choose $Al^{3+}$ to act as the promising dopant in NiO nanocrystals for optimizing the gas sensing properties of NiO-based gas sensor. The pure and various Al doping amounts of NiO nanorod-flowers were prepared to compare and evaluate the structural features and sensing characteristics aiming to examine the best Al doping amount and the effect of $Al^{3+}$ in the NiO nanomaterial on the gas sensing properties.

## EXPERIMENTAL SECTION

**Preparation of the Pure and Al-Doped NiO Nanorod-Flowers.** The pure NiO nanorod-flowers were prepared by a solvothermal reaction. In a typical procedure, of Al $(NO_3)_3 \cdot 9H_2O$ and 0.582 g Ni $(NO_3)_2 \cdot 4H_2O$ were dissolved in in a mixed solution containing 10 mL of deion-

ized water and 15 mL of ethylene glycol with constantly stirring to form a clear solution. Then, 0.126 g $H_2C_2O_4$•$2H_2O$ was added into the above solution. After that the solution was transferred into a 40 mL Teflon-lined stainless-steel autoclave and heated at 120 °C for 12 h. After the autoclave was cooled down to room temperature, the resulting products were collected and washed with deionized water and ethanol by centrifugation several times, and then dried at 80 °C in air for 24 h. Finally, the undoped NiO nanorod-flowers were obtained by annealing above products at 450 °C for 2 h in air. The synthetic process of Al-doped NiO nanorod-flowers was similar to the above procedure except adding various amounts of Al $(NO_3)_3$•$9H_2O$ (Al/Ni=2, 5, 8, and 10 at%) in reaction solution. The Al compositions of the Al-doped NiO samples prepared from the solutions with the ratios of 2, 5, 8, and 10 at% were determined to be 0.59, 1.45, 2.15, and 3.04 at%, respectively, by inductively coupled plasma mass spectroscopy.

**Characterization.** The X-ray diffraction (XRD) patterns were collected by using Rigaku TTRIII X-ray diffractometer operated at 40 kV and 200 mA with Cu Kα radiation at a wavelength of 1.5406 Å. The size and morphology of the samples were investigated by JSM-7500F (JEOL) microscope operating at 15 kV and JEM-2200FS (JEOL) operating at 200 kV. The energy dispersive X-ray spectroscopic (EDS) elemental mapping and spectrum were investigated by the TEM attachment. The X-ray photoelectron spectroscopy (XPS) measurements were performed with Mg-Kα X-ray source (1253.6 eV Specs XR50). The doping concentration of Al in various Al-doped NiO samples was determined by inductively coupled plasma-atomic emission spectroscopy (ICP-AES, OPTIMA 3300DV).

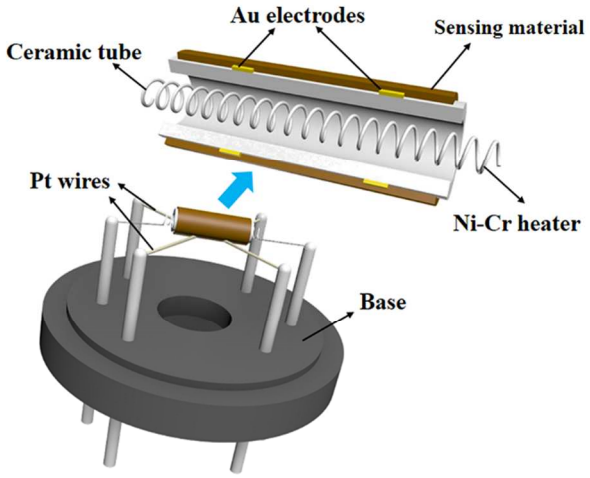


Figure 1. Schematic diagram of the gas sensor.

**Fabrication and Measurement of Gas Sensor.** The schematic of the fabricated gas sensor is shown in Figure 1 and the fabrication process is described as follow: First the undoped and Al-doped NiO samples were dispersed in deionized water to form a paste. Then the paste was coated on an alumina tube (length: 4 mm, external diameter: 1.2 mm, and internal diameter: 0.8 mm; a pair of Au electrodes were installed at the end of the tube, and each electrode was connected with a pair of Pt wires) to form a thick sensing film. The thickness of the sensing film was ~38.8 μm (Figure S1). Subsequently, the resulted sensing device was sintered at 400 °C for 2 h. Finally, a Ni-Cr alloy coil as a heater was inserted to the alumina tube so that the operating temperature can be controlled by adjusting the heating current flowed through the heater. The gas sensing performance of the gas sensor was evaluated by a static test method using RQ-2 gas-sensing characterization system. The electrical resistance of the sensor in different environmental atmospheres was measured and the atmospheric air was used as the referenced gas. The gas response (S) of the sensors is defined as the ratio of $R_g/R_a$, which $R_g$ and $R_a$ are the electrical resistance of the sensors in the target gases and atmospheric air. The response and recovery times are defined as the time taken for achieving 90% of the total resistance changes after the sensor was exposed to the target gases and atmospheric air, respectively.

## RESULTS AND DISCUSSION

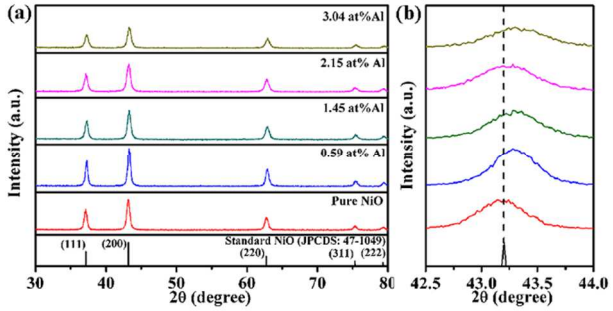


Figure 2. (a) Full angel range of XRD patterns and (b) high-resolution of (200) peak of the pure, 0.59 at%, 1.45 at%, 2.15 at%, and 3.04 at% Al-doped NiO nanorod-flowers.

**Structural and Morphological Characteristics.** The XRD patterns of the pure and Al-doped NiO samples are shown in Figure 2a. Clearly, all the diffraction peaks of all the samples could be indexed to the face-centered cubic NiO phase (JCPDS No. 47-1049). No other peaks corresponding to Al-related compounds were observed in all the XRD patterns of 0.59-3.04 at% Al-doped NiO samples. In addition, as shown in Figure 2b, a high angle shift was detected from the (200) peak via comparing the Al-doped NiO with pure NiO. This could be ascribed to the difference between the radii of $Ni^{2+}$ and $Al^{3+}$. The radius of $Ni^{2+}$ at the coordination number of 6 was 0.69 Å, which was larger than that of $Al^{3+}$ (0.54 Å) at the same coordination number. Therefore, the substitution of $Ni^{2+}$ by $Al^{3+}$ induced the high angle shift of diffraction peaks, confirming that $Al^{3+}$ is incorporated into the NiO lattice. Moreover, the average crystallite sizes of the pure, 0.59 at%, 1.45 at%, 2.15 at%, and 3.04 at% Al-doped NiO samples calculated by Scherrer formula were about 22.7, 21.8, 15.1, 13.5, and 11.9 nm respectively, which indicated that the addition of Al could effectively prevent NiO crystallites from further growing-up.

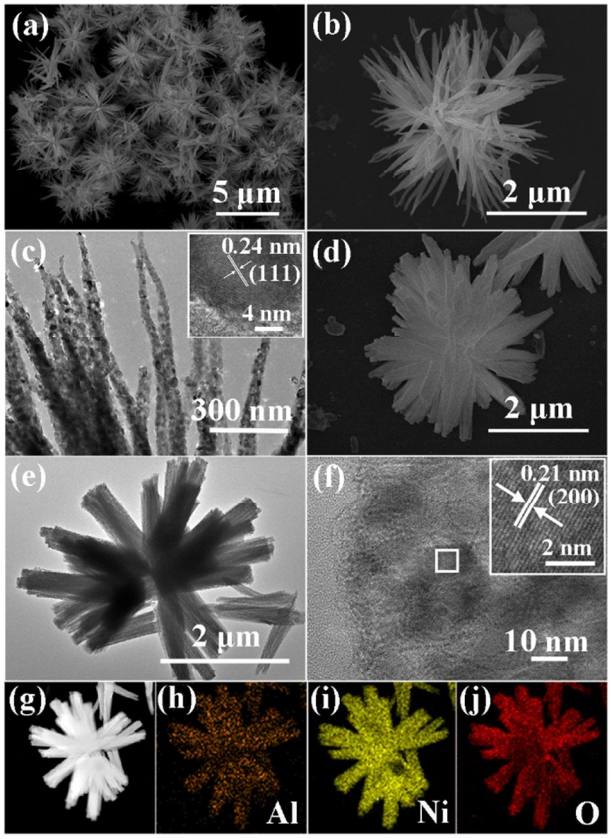


Figure 3. (a-c) Typical FESEM, TEM and HRTEM images of the pure NiO nanorod-flowers. (d-f) The FESEM, TEM and HRTEM images of the 2.15 at% Al-doped NiO nanorod-flowers. (g-j) Scanning TEM (STEM) image and the corresponding energy dispersive X-ray spectroscopic (EDS) elemental mapping images of the 2.15 at% Al-doped NiO nanorod-flowers.

The morphologies of the as-prepared pure and Al-doped NiO samples were examined by FESEM and TEM. Figure 3a depicts the low-magnification FESEM image of the pure NiO, from which a number of nanorod-flowers with uniform size and good dispersity were clearly observed. The average diameter of the nanorod-flower was about 4 μm. The enlarged SEM image in Figure 3b provides a single NiO nanorod-flower, it could be found that the nanorod-flower was composed of many needle-like nanorods. Further observing in the TEM image of Figure 3c, the nanorods were assembled by numerous nanoparticles. Moreover, the inset of Figure 3c shows a high-resolution TEM (HRTEM) image of NiO nanoparticles, which confirms that the NiO nanoparticles were single crystalline. The clear lattice fringe with the lattice spacing of 0.24 nm was well corresponded to the (111) plane of cubic NiO.

After incorporating a small trace of $Al^{3+}$ into NiO crystals, the nanorod-flower morphologies of as-synthesized Al-doped NiO samples were maintained. Figure 3d shows the typical FESEM images of an individual 2.15 at% Al-doped NiO nanorod-flower. The single 0.59 at%, 1.45 at%, and 3.04 at% Al-doped NiO nanorod-flowers are displayed in Figure S2a-c. It was clear that the needle-like nanorods became thicker with the increase of Al doping amount, although all the Al-doped NiO nanorod-flower had the similar sizes. The panoramic FESEM images of the 0.59-3.04 at% Al-doped NiO nanorod-flowers are also shown in Figure S3a-d, which revealed the well-dispersed morphological features. TEM and HRTEM were employed to further investigate the structural features of the Al-doped NiO nanorod-flowers. Typically, the 2.15 at% Al-doped NiO sample was chosen to examine. As shown in Figure 3e, the size and morphology of the 2.15 at% Al-doped NiO sample were similar to what we had been observed in FESEM images. The HRTEM image (Figure 3f) displays clear lattice fringer with spacing of 0.21 nm, which could be attributed to the (200) lattice planes of NiO. Furthermore, the EDS elemental mapping analysis was adopted to confirm the composition of the 2.15 at% Al-doped NiO nanorod-flower. Figure 3g shows the scanning TEM (STEM) image of a single 2.15 at% Al-doped NiO nanorod-flower. Figure 2h-j depict the spatial distribution of Al, Ni, and O, respectively. Obviously, all the three kinds of elements were detected and distrubuted uniformly in the region of nanorod-flower. Moreover, the Al signal was much weaker than the Ni and O signals, which indicated that the content of Al was much lower than that of Ni and O.

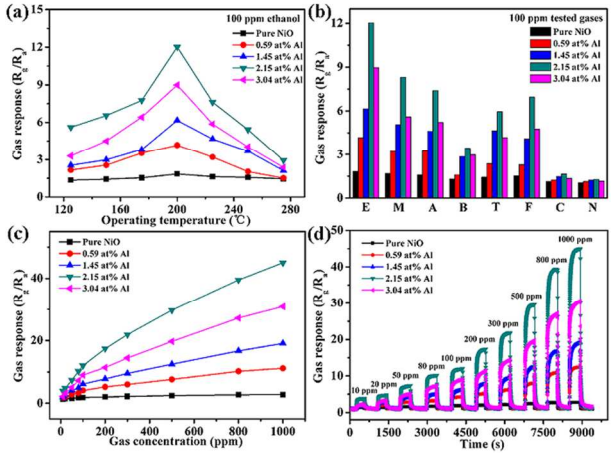


Figure 4. (a) The gas responses of the sensors based on the pure, 0.59 at%, 1.45 at%, 2.15 at%, and 3.04 at% Al-doped NiO nanorod-flowers vs operating temperatures to 100 ppm ethanol. (b) The gas responses of five sensors to 100 ppm various target gases (E, ethanol; M, methanol; A, acetone; B, benzene; T, toluene; F, formaldehyde; C, CO; N, $NH_3$) at 200 °C. (c) The gas responses of five sensors as the function of the ethanol concentration at 200 °C. (d) The real-time response curves of five sensors to different ethanol concentration at 200 °C.

**Gas Sensing Properties.** In order to demonstrate that the doping of Al into NiO nanorod-flowers is an effective way to enhance the gas sensing properties of NiO-based gas sensor, the gas sensing performances of the sensors based on the pure and various Al doping amount of NiO nanorod-flowers were investigated. Firstly, the gas responses of the sensors based on the pure, 0.59 at%, 1.45 at%, 2.15 at%, and 3.04 at%

Al-doped NiO samples to 100 ppm ethanol were measured at different operating temperatures from 125 °C to 275 °C to explore the optimal Al doping amount as well as the relationship between gas response and operating temperature, as shown in Figure 4a. Obviously, the volcano-shaped correlation between gas response and operating temperature was observed for all the samples and the optimal operating temperature of every sample was 200 °C. Meanwhile, the gas response was greatly improved due to Al doping. The gas responses of the sensors based on the pure, 0.59 at%, 1.45 at%, and 3.04 at% Al-doped NiO to 100 ppm ethanol at 200 °C were 1.9, 4.2, 6.2, 12.0, and 8.9, respectively. The result revealed that the sensor based on 2.15 at% Al-doped NiO showed the highest response to 100 ppm ethanol and the value was about 6.3 times higher than that of the pure NiO.

Subsequently, the gas responses of five sensors to 100 ppm various target gases at 200 °C were tested. The target gases included ethanol, methanol, acetone, benzene, toluene, formaldehyde, CO, and NH3. As shown in Figure 4b, all the Al-doped NiO samples displayed enhanced responses for each target gas compared with the pure NiO. Moreover, the response of all the sensors to ethanol was clearly higher than that to other gases. Especially, the sensor based on 2.15 at% Al-doped NiO had the strongest response to ethanol and the value was about 1.5~7.2 times higher than other target gases, while ratio was only about 1.1~1.8 for the pure NiO. This result testified that the doping of Al into NiO improved the selectivity of the NiO-based sensor to ethanol.

Figure 4c shows the responses of five gas sensors as the function of the ethanol concentration at 200 °C. It could be observed that the response increased with increasing the ethanol concentration from 10 to 1000 ppm for all five sensors, and the growth gradually slowed down. Among them, the response of the sensor based on the 2.15 at% Al-doped NiO was apparently higher than that of the pure, 0.59 at%, 1.45 at%, and 3.04 at% Al-doped NiO to various ethanol concentration we tested. Moreover, we could find that the response of the sensor based on the 2.15 at% Al-doped NiO did not tend to saturation gradually when the ethanol concentration was raised to 1000 ppm, although the increasing trend slowed down with the increase of the ethanol concentration. This indicated that the 2.15 at% Al-doped NiO based gas sensor had the wide test range. In addition, the real-time response curves of five sensors to different ethanol concentration at 200 °C are displayed in Figure 4d. The result showed that all the sensors exhibited excellent response and recovery characteristics with respect to different ethanol concentration ranging from 10 to 1000 ppm.

From these, the Al doping amount of 2.15 at% was considered as the optimum doping concentration. Then the response and recovery characteristics of the sensor based on 2.15 at% Al-doped NiO nanorod-flowers were investigated to 100 ppm ethanol at 200 °C. As shown in Figure S4, the resistance increased upon exposure to ethanol, which was consistent with the gas sensing behavior of p-type oxide semiconductor. The response and recovery times of the sensor based on the 2.15 at% Al- doped NiO were 48 s and 40 s, respectively. The relatively rapid response and recovery contribute to the real-time detection of ethanol gas.

A comparison of the sensing performances between the sensor in this work and other ethanol sensors based on NiO reported previously in the literatures is summarized in Table 1. From the table, comprehensively considering the gas response and operating temperature, it is obvious that 2.15 at% Al-doped NiO nanorod-flowers showed relatively high gas response and low operating temperature. This was conductive to practical application and energy conservation. Therefore, the sensor based on 2.15 at% Al-doped NiO nanorod-flowers had more superiority than those reported in the literatures.[26, 28-31]

**Gas Sensing Mechanism.** It is well known that the gas sensing properties are primarily effected by the electrical conductivity and the surface chemisorbed oxygen species of the sensing materials. Thus, the investigation of carrier concentration and distribution of oxygen component in the sensing materials is extremely necessary. Here, XPS analysis was adopted to explore the possible mechanism for enhanced gas sensing properties of Al-doped NiO nanorod-flowers. Figure S3a shows the XPS survey spectrum of the 2.15 at% Al-doped NiO nanorod-flowers, in which the signals of Ni and Al could be clearly observed. The Al 2p spectrum is illustrated in Figure S3b, from which the peak located at 73.9 eV was assigned to $Al^{3+}$.[32] Figure 5a and b show the high resolution scans of the pure and 2.15 at% Al-doped NiO nanorod-flowers for Ni $2p_{3/2}$. It could be found that $Ni^{2+}$ and $Ni^{3+}$ bonding energies were clearly observed at 854.5 and 855.0 eV for the pure NiO, as well as 856.4 and 856.8 eV for the 2.15 at% Al-doped NiO. Fur-

**Table 1** Comparison of the sensing performances between the current work and previously reported results[26, 28-31]

| Sensing materials | Ethanol concentration (ppm) | Temperature (°C) | Gas response ($R_g/R_a$) | Reference |
|---|---|---|---|---|
| 3.04 at% Fe-doped NiO nanofibers | 100 | 450 | 245.0 | 26 |
| Fe-doped ordered mesoporous NiO | 100 | 240 | 4.8 | 28 |
| $WO_3$•0.33$H_2O$-NiO composite | 100 | 280 | 3.9 | 29 |
| NiO/multi-wall carbon nanotubes | 100 | 180 | 2.0 | 30 |
| Flower-like NiO microspheres | 100 | 250 | 3.2 | 31 |
| 2.15 at% Al-doped NiO nanorod-flowers | 100 | 200 | 12.0 | This work |

thermore, from Figure 5a, the $Ni^{3+}/Ni^{2+}$ ratio was determined to be 0.77 in the pure NiO. However, the $Ni^{3+}/Ni^{2+}$ ratio increased to 1.34 when 2.15 at% of $Al^{3+}$ was doped into NiO nanocrystals (Figure 5b). A higher energy shift and an increase of the $Ni^{3+}/Ni^{2+}$ ratio were verified.

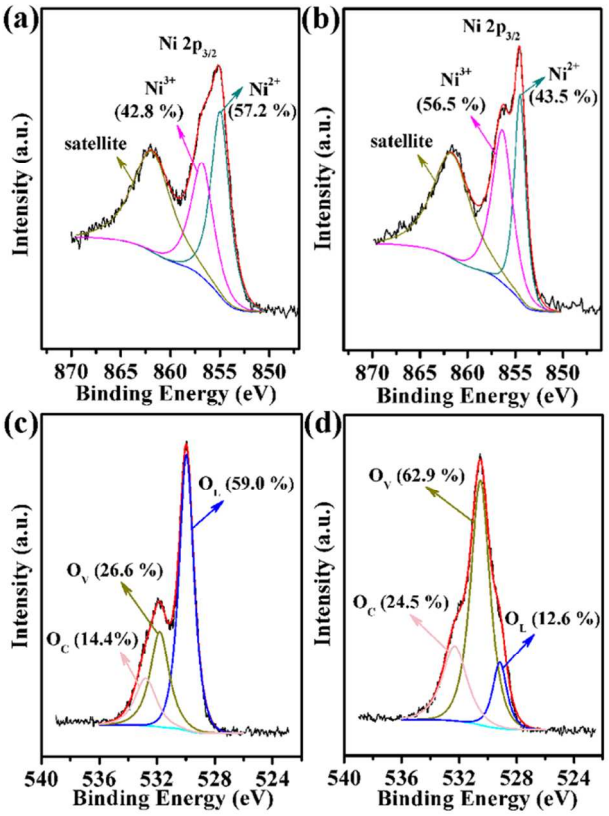


Figure 5. (a and b) Ni $2p_{3/2}$ XPS spectra of the pure and 2.15 at% Al-doped NiO nanorod-flowers. (c and d) O 1s XPS spectra of the pure and 2.15 at% Al-doped NiO nanorod-flowers.

It is reported that $Ni^{3+}$ can be formed from adsorbing negatively charged oxygen on the surface of NiO and/or caused by negatively charged interstitial oxygen ($O_i''$).[33, 34] The substitution of $Al^{3+}$ at the site of $Ni^{2+}$ can be compensated by the electronic compensation mechanism, which is described as follows:

$$Al_2O_3 \xrightarrow{2NiO} 2Al_{Ni}^{\bullet} + 2e' + 2O_O^{\times} + \frac{1}{2}O_2(g) \quad (1)$$

According to the Eq. (1), the oxygen molecules are generated by the incorporation reaction. Therefore, the oxygen molecules generated from Eq. (1) will convert into negatively charged interstitial (or surface) oxygen through the oxidation of $Ni^{2+}$ into $Ni^{3+}$ (Eq. (2)).

$$\frac{1}{2}O_2(g) + 2NiO \xrightarrow{2NiO} O_i'' + 2Ni_{Ni}^{\bullet} + 2O_O^{\times} \quad (2)$$

From the above, the increase of $Ni^{3+}/Ni^{2+}$ caused by the partial oxidation of $Ni^{2+}$ to $Ni^{3+}$ means $Al^{3+}$ was incorporated into the NiO lattice. As described in Eq. (1), with the substitution of $Al^{3+}$ at $Ni^{2+}$ sites, electrons are generated to compensate for substituting $Al^{3+}$ into $Ni^{2+}$ sites, which decrease the hole concentration in NiO. It also could be supported by the increase of $R_a$ with raising the Al-doping amount (Figure S6). The change in hole concentration may be the key factor for the enhanced gas response. It has also reported that when the hole concentration is very low, the injection of the equal amounts of electrons by the sensing reaction between ethanol molecules and chemisorbed oxygen ions will lead to a higher variations in sensor resistance, and thus enhance the gas response.[26, 35]

What's more, the O 1s peaks were asymmetric and could be fitted into three different components.[36] The binding energy at about 529.5 ± 0.4 eV ($O_L$), 531.2 ± 0.6 eV ($O_V$), and 532.5 ± 0.2 eV ($O_C$) were attributed to lattice oxygen, oxygen-deficient regions, and chemisorbed oxygen species, respectively. The relative percentages of $O_L$, $O_V$, and $O_C$ components were approximately 59.0, 26.6, and 14.4 % in the pure NiO, while those were 12.6, 62.9, and 24.5 % in the 2.15 at% Al-doped NiO. Apparently, with Al doping, the contents of $O_V$ and $O_C$ components were greatly increased. This indicated that the gas sensing properties were closely related to the deficient and chemisorbed oxygen in NiO material. The increase of $O_V$ component could provide more active sites for the gas reaction and adsorption on the surface of the sensing materials. The rise of $O_C$ component means that more surface chemisorbed oxygen species could participate in the oxidation-reduction reaction occurred on the surface of the sensing materials and thus caused a larger change in sensor resistance.

## CONCLUSION

In summary, we successfully synthesized the pure and Al-doped NiO nanorod-flowers with well-dispersed hierarchical nanostructures and uniform sizes by the solution-based route. In gas sensing applications, a systematically comparative analyse indicated that the 2.15 at% Al-doped NiO nanorod-flowers showed the greatly enhanced gas sensing performance compared to the pure NiO nanorod-flowers. The changes of the carrier concentration and distribution of oxygen component induced by the incorporation of $Al^{3+}$ with NiO nanocrystals were responsible for the enhanced gas sensing performance. Hence, we can confirm that the doping of $Al^{3+}$ into NiO nanorod-flowers is a promising strategy for improving the gas sensing performance of the NiO-based gas sensor.

## ASSOCIATED CONTENT

**Supporting Information**. FESEM image of the section of a fabricated sensor; FESEM images of the single 0.59 at%, 1.45 at%, and 3.04 at% Al-doped NiO nanorod-flower; The panoramic FESEM images of the 0.59 at%, 1.45 at%, 2.15 at% and 3.04 at% Al-doped NiO nanorod-flowers; Response and recovery characteristics of the sensor based on the 2.15 at% Al-doped NiO nanorod-flowers to 100 ppm ethanol at 200 °C; The XPS spectra of the 2.15 at% Al-doped NiO nanorod-flowers: a survey scan, and Al 2p; The dependence of the resistances in air on the doping amount of Al for the sensors at different temperature. This material is available free of charge via the Internet at http://pubs.acs.org.

## AUTHOR INFORMATION

### Corresponding Author

* Tel: +86-431-85167808. Fax: +86-431-85167808. E-mail addresses: spmaster2008@163.com (Peng Sun), lugy@jlu.edu.cn (Geyu Lu).

### Notes

The authors declare no competing financial interest.

## ACKNOWLEDGMENT

This work is supported by the National Nature Science Foundation of China (Nos. 61374218, 61134010, and 61327804), the Program for Chang Jiang Scholars and Innovative Research Team in University (No. IRT13018), the National High-Tech Research and Development Program of China (863 Program, Nos. 2013AA030902 and 2014AA06A505), and Project 2015094 supported by the Graduate Innovation Fund of Jilin University.

## ABBREVIATIONS

MOS, metal oxide semiconductor; VOC, volatile organic compounds; XRD, X-ray diffraction; FESEM, field-emission electron scanning microscopy; TEM, transmission electron microscopy; EDS, energy dispersive X-ray spectroscopy; XPS, X-ray photoelectron spectroscopy; HRTEM, high-resolution transmission electron microscopy; STEM, scanning transmission electron microscopy; ICP-AES, inductively coupled plasma-atomic emission spectroscopy.

## REFERENCES

(1) Kim, I.-D.; Rothschild, A.; Tuller, H. L.; Liewhiran, C. Advances and New Directions in Gas-Sensing Devices. Acta Mater. 2013, 61, 974-1000.
(2) Wangner, T.; Haffer, S.; Weinberger, C.; Klaus, D.; Tiemann, M. Mesporous Materials as Gas Sensors. Chem. Soc. Rev. 2013, 42, 4036-4053.
(3) Das, S.; Jayaraman, V. $SnO_2$: A Comprehensive Review on Structures and Gas Sensors. Prog. Mater. Sci. 2014, 66, 112-255.
(4) Afzal, A.; Cioffi, N.; Sabbatini, L.; Torsi, L. $NO_x$ Sensors Based on Semiconducting Metal Oxide Nanostructures: Progress and Perspectives. Sens. Actuators, B 2012, 171, 25-42.
(5) Korotcenkov, G. Metal Oxides for Solid-State Gas Sensors: What Determines Our Choice? *Mater. Sci. Eng., B* 2007, 139, 1-23.
(6) Barsan, N.; Koziej, D.; Weimar, U. Metal Oxide-Based Gas Sensor Research: How to? Sens. Actuators, B 2007, 121, 18-35.
(7) Yamazoe, N.; Sakai, G.; Shimanoe, K. Oxide Semiconductor Gas Sensors. Catal. Sury. Asia 2003, 7, 63-75.
(8) Korotcenkov, G. The Role of Morphology and Crystallographic Structure of Metal Oxides in Response of Conductometric-Type Gas Sensors. Mater. Sci. Eng., R 2008, 61, 1-39.
(9) Lee, J.-H. Gas Sensors Using Hierarchical and Hollow Oxide Nanostructures: Overview. Sen. Actuators, B 2009, 140, 319-336.
(10) Comini, E. Metal Oxide Nano-Crystals for Gas Sensing. Anal. Chim. Acta 2006, 568, 28-40.
(11) Wang, S.; Xiao, B.; Yang, T.; Wang, P.; Xiao, C.; Li, Z.; Zhao, R.; Zhang, M. Enhanced HCHO Gas Sensing Properties by Ag-Loaded Sunflower-Like $In_2O_3$ Hierarchical Nanostructures. J. Mater. Chem. A 2014, 2, 6598-6604.
(12) Bao, M.; Chen, Y.; Li, F; Ma, J.; Lv, T.; Tang, Y.; Chen, L.; Xu, Z.; Wang, T. Plate-Like P-N Heterogeneous NiO/$WO_3$ Nanocomposites for High Performance Room Temperature $NO_2$ Sensors. Nanoscale 2014, 6, 4063-4066.
(13) Kim, H.-J.; Yoon, J.-W.; Choi, K.-I.; Jang, H. W.; Umar, A.; Lee, J.-H. Ultraselective and Sensitive Detection of Xylene and Toluene for Monitoring Indoor Air Pollution Using Cr-Doped NiO Hierarchical Nanostructures. Nanoscale 2013, 5, 7066-7073.
(14) Cheng, J. P.; Wang, B. B.; Zhao, M. G.; Liu, F.; Zhang, X. B. Nickel-Doped Tin Oxide Hollow Nanofibers Prepared by Electrospinning for Acetone Sensing. Sen. Actuators, B 2014, 190, 78-85.
(15) Flynn, C. J.; Oh, E. E.; McCullough, S. M.; Call, R. W.; Donley, C. L.; Lopez, R.; Cahoon, J. F. Hierarchically-Structured NiO Nanoplatelets as Mesoscale P-Type Photocathodes for Dye-Sensitized Solar Cells. J. Phys. Chem. C 2014, 118, 14177-14184.
(16) Choi, S. H; Kang, Y. C. Ultrafast Synthesis of Yolk-Shell and Cubic NiO Nanopowders and Application in Lithium Ion Batteries. ACS Appl. Mater. Interfaces 2014, 6, 2312-2316.
(17) Wei, Z. P.; Arredondo, M.; Peng, H. Y.; Zhang, Z.; Guo, D. L.; Xing, G. Z.; Li, Y. F.; Wong, L. M.; Wang, S. J.; Valanoor, N.; Wu, T. A Template and Catalyst-Free Metal-Etching-Oxidation Method to Synthesize Aligned Oxide Nanowire Arrays: NiO as an Example. ACS nano 2010, 4, 4785-4791.
(18) Song, X. F; Gao, L.; Mathur, S. Synthesis, Characterization, and Gas Sensing Properties of Porous Nickel Oxide Nanotubes. J. Phys. Chem. C 2011, 115, 21730-21735.
(19) Wang, J.; Wei, L.; Zhang, L. J.; Jiang, C.; Kong, E. S.-W.; Zhang, Y. Preparation of High Aspect Ratio Nickel Oxide Nanowires and Their Gas Sensing Devices with Fast Response and High Sensitivity. *J. Mater. Chem.* 2012, 22, 8327-8335.
(20) Sun, P.; Mei, X.; Cai, Y.; Ma, J.; Sun, Y.; Liang, X.; Liu, F.; Lu, G. Synthesis and Gas Sensing Properties of Hierarchical $SnO_2$ Nanostructures. Sen. Actuators, B 2013, 187, 301-307.
(21) Lai, H.-Y.; Chen, T.-H.; Chen, C.-H. Architecture Controlled Synthesis of Flower-Like $In_2O_3$ Nanobundles with Significantly Enhanced Ultraviolet Scattering and Ethanol Sensing. *CrystEngComm* 2012, 14, 5589-5595.
(22) Hieu, H. N.; Vuong, N. M.; Jung, H.; Jang, D. M.; Kim, D.; Kim, H.; Hong, S.-K. Optimization of a Zinc Oxide Urchin-Like Structure for High-Performance Gas Sensing. *J. Mater. Chem.* 2012, 22, 1127-1134.
(23) Wang, C.; Sun, R.; Li, X.; Sun, Y.; Sun, P.; Liu, F.; Lu, G. Hierarchical Flower-Like $WO_3$ Nanostructures and Their Gas Sensing Properties. Sen. Actuators, B 2014, 204, 224-230.
(24) Bai, G.; Dai, H.; Deng, J.; Liu, Y.; Ji, K. Porous NiO Nanoflowers and Nanourchins: High Active Catalysts for Toluene Combustion. *Catal. Commun.* 2012, 27, 148-153.
(25) Bai, G.; Dai, H.; Deng, J.; Liu, Y.; Qiu, W.; Zhao, Z.; Li, X.; Yang, H. The Microemulsion Preparation and High Catalytic Performance of Mesoporous NiO Nanorods and Nanocubes for Toluene Combustion. Chem. Eng. J. 2013, 219, 200-208.
(26) Yoon, J.-W.; Kim, H.-J.; Kim, I.-D.; Lee, J.-H. Electronic Sensitization of the Response to $C_2H_5OH$ of P-Type NiO Nanofibers by Fe Doping. Nanotechnology, 2013, 24, 44405-44412.
(27) Wang, C.; Liu, J.; Yang, Q.; Sun, P.; Gao, Y.; Liu, F.; Zheng, J.; Lu, G. Ultrasensitive and Low Detection Limit of Acetone Gas Sensor Based on W-Doped NiO Hierarchical Nanostructure. Sen. Actuators, B 2015, 220, 59-67.
(28) Sun, X.; Hu, X.; Wang, Y.; Xiong, R.; Li, X.; Liu, J.; Ji, H.; Li, X.; Cai, S.; Zheng, C. Enhanced Gas-Sensing Performance of Fe-Doped Ordered Mesoporous NiO with Long-Range Periodicity. J. Phys. Chem. C 2015, 119, 3228-3237.
(29) Lin, L.; Liu, T.; Zhang, Y.; Hussain, S.; Wu, S.; Zeng, W. Superior Ethanol-Sensing Performance Research of $WO_3$•0.33$H_2O$ Doped Chrysanthemum-Like NiO Composite. Mater. Lett. 2013, 108, 231-234.
(30) Chen, N.; Li, Q.; Li, Y.; Deng, D.; Xiao, X.; Wang, Y. Facile Synthesis and Gas Sensing Performances Based on Nickel Oxide Nanoparticles/Multi-Wall Carbon Nanotube Composite. J. Mater. Sci.: Mater. Electron. 2015, 26, 8240-8248.
(31) San, X.; Wang, G.; Liang, B.; Ma, J.; Meng, D.; Shen, Y. Flower-Like NiO Hierarchical Microspheres Self-Assembled with

Nanosheets: Surfactant-Free Solvothermal Synthesis and Their Gas Sensing Properties. J. Alloys Compd. 2015, 636, 357-362.
(32) Gao, D.; Zhang, J.; Yang, G.; Zhang, J.; Shi, Z.; Qi J,; Zhang, Z.; Xue, D. Ferromagnetism in ZnO Nanoparticles Induced by Doping of A Nonmagnetic Element: Al. J. Phys. Chem. C 2010, 114, 13477-13481.
(33) Kohl, D. Function and Applications of Gas Sensors. J. Phys. D: Appl. Phys. 2001, 34, R125.
(34) Yang, M.; Pu, H.; Zhou, Q.; Zhang, Q. Transparent P-type Conducting K-Doped NiO Films Deposited by Pulsed Plasma Deposition. Thin Solid Films 2012, 520, 5884-5888.
(35) Kim, H.-J; Jeong, H.-M.; Kim, T.-H.; Chung, J.-H.; Kang, Y. C.; Lee, J.-H. Enhanced Ethanol Sensing Characteristics of $In_2O_3$-Decorated NiO Hollow Nanostructures via Modulation of Hole Accumulation Layers. ACS Appl. Mater. Interfaces 2014, 6, 18197-18204.
(36) Alenezi, M. R.; Alshammari, A. S.; Jayawardena, K. D. G. I.; Beliatis, M. J.; Henley, S. J.; Silva, S. R. P. Role of The Exposed Polar Facets in The Performance of Thermally and UV Activated ZnO nanostructured Gas Sensors. J. Phys. Chem. C 2013, 117, 17850-17858.

Table of Contents